Shape Constrained Automatic Segmentation of the Liver based on a Heuristic Intensity Model

Dagmar Kainmüller[1], Thomas Lange[2], and Hans Lamecker[1]

[1] Zuse Institute Berlin, Germany, {kainmueller,lamecker}@zib.de
[2] Charité Berlin, Germany, thomas.lange@charite.de

Abstract. We present a fully automatic 3D segmentation method for the liver from contrast-enhanced CT data. It is based on a combination of a constrained free-form and statistical deformable model. The adaptation of the model to the image data is performed according to a simple model of the typical intensity distribution around the liver boundary and neighboring anatomical structures, considering the potential presence of tumors in the liver. All parameters of the deformation as well as the initial positioning of the model in the data are estimated automatically.

1 Introduction

The main issue in automatic liver segmentation from contrast-enhanced CT data is that the intensity values of the liver tissue are often similar to those of some surrounding anatomical structures like stomach, pancreas, kidney and muscles. Approaches which are only based on local intensity or intensity gradient features are usually not sufficient to differentiate between liver tissue and other anatomical structures in those regions.

In order to alleviate this problem prior knowledge about the typical shape of a liver may be incorporated into the process to constrain the segmentation process where the image information is not reliable. The shape may be constrained by a single template [1], a statistical shape model (SSM) [2] or even more flexible deformable models. Combinations of these approaches have also been presented [3, 4]. In this work we adopt a combination of a constrained free-form and a statistical deformable model, which will be explained in Sec. 2.1.

Just as important and challenging is the process that drives the model to match the image data to be segmented. General intensity features [1, 3] or a statistical model of the intensity distribution [5] have been used. In this work we present a simple heuristic model of the typical intensity distribution around the liver boundary based on a nonlinear isotropic diffusion filtering of the original CT data. The model also considers the potential presence of tumors inside the liver. An algorithm for computing displacement vectors is derived that drives the surface deformation (see Sec. 3). This model extends previous work [6, 7].

In order to achieve fully automatic segmentation both the set of parameters required for the computation of the displacements as well as the initial positioning of the model in the image data need to be estimated automatically from the image data. Our solutions for these problems are presented in Sec. 4 and Sec. 5.

T. Heimann, M. Styner, B. van Ginneken (Eds.): 3D Segmentation in The Clinic:
A Grand Challenge, pp. 109-116, 2007.

2 Deformable Model based Segmentation Framework

2.1 Statistical Shape Model driven Segmentation

The SSM used in this work is generated from a set of individual training shapes (triangulated surfaces). The main challenge is the correct identification of anatomically corresponding points on each training surface. The method described in [6, 7] was adopted to generate the shape model of the liver (see also for a review of other methods). As a result of this process all training shapes v_i $(i = 1, \ldots, n)$ can be represented in a common vector space $\mathbb{R}^{3m}$, with m the number of sample points used to discretize the shapes (vertices of the surfaces). Principal component analysis (PCA) on this set of vectors provides a compact representation of the variability within the training set, resulting in a bi-linear model:

$$S(b, T) = T\left(\overline{v} + \sum_{k=1}^{n-1} b_k p_k\right) \tag{1}$$

where $\overline{v} = \sum v_i/n$ is the average shape, $p_k \in \mathbb{R}^{3m}$ the eigenmodes of the covariance matrix $C = \sum (v_i - \overline{v})(v_i - \overline{v})^T/n$. The shape weights $b \in \mathbb{R}^{n-1}$ and the linear transformation T constitute the degrees of freedom of the model.

Segmentation using the SSM (1) is the task of finding the set of position and shape parameters such that $S(b, T)$ approximates the (unknown) shape $R \in \mathbb{R}^{3m}$ to be segmented as good as possible. We denote the optimal segmentation $R^* = S(b^*, T^*)$. However, the location and shape of R is only encoded implicitly in the image data $I : \mathbb{R}^3 \to \mathbb{R}$. Therefore the computation of R^* proceeds iteratively. Let $R^i = S(b^i, T^i)$ denote the segmentation in iteration i:

1. $R^0 := S(0, T^0)$. The computation of T^0 is described in Sec. 5.
2. Compute *displacement* vector field $\Delta R \in \mathbb{R}^{3m}$ defined on the current segmentation R^i, i.e. a vector $\Delta r_k \in \mathbb{R}^3$ is assigned to each vertex $k \in \mathbb{N}$ of the surface R^i. It describes the desired deformation of the model towards the (unknown) surface R in the underlying image data I (see Sec. 3).
3. Project the displacements onto the SSM by solving the optimization problem $(b^{i+1}, T^{i+1}) = \operatorname{argmin}_{b,T} |(R^i + \Delta R) - S(b, T)|^2$. Note that this process may in general introduce self-intersections of the surface.
4. Update $i \leftarrow i + 1$ and return to step (2) if convergence has not been achieved, i.e. if $|S(b^i, T^i) - S(b^{i+1}, T^{i+1})| > 3m \cdot \epsilon$; else return $b^* = b^i$ and $T^* = T^i$.

It is not clear how well the final solution R^* approximates R. This depends on the quality of the shape model, the nature of the iterative approach and on the computation of ΔR^i. In order to compute the displacement vector field ΔR^i an *intensity model* for the encoding of R in I must be established. Our model will be described in detail in Sec. 3.

2.2 Constrained Free-Form Segmentation

Although the SSM based segmentation provides robustness it may lack flexibility to accurately model the desired segmentation R. To overcome this limitation we

perform a so called *free form segmentation* step, starting from the previous result R^*. However, we constrain the free form segmentation to a narrow band around R^* to prevent too large deviations from the prior shape. The free form segmentation is performed as follows:

1. $R^0 := R^*$.
2. Compute three different vector fields on the current segmentation R^i: A *displacement* vector field ΔR, just as in Sec. 2.1, a *smoothing* vector field ΔS, pulling each vertex towards the barycenter of its 1-ring neighborhood, and a *shape preserving* vector field ΔP, moving each vertex that lies outside a narrow band of radius r_B around R^* along the surface normal towards the inside.
3. Compute a *resulting* vector field ΔV. For an individual vertex of the surface it is given by $v = w_r \Delta r + w_s \Delta s + w_p \Delta p$. The weights depend on the cosines $c_{ab} = \cos(\angle(\Delta a, \Delta b))$ with $a, b \in \{s, r, p\} (a \neq b)$ as follows:
   (1) $|\Delta p| > 0 \Rightarrow w_s := 0.15 \cdot (1 - c_{ps})$, $w_r := 0$, $w_p := 1 - w_s$.
   (2) $|\Delta p| = 0 \Rightarrow w_s := 0.15 \cdot (1 - c_{pr})$, $w_r := 1 - w_s$, $w_p := 0$.
   (3) For $a, b \in \{s, r, p\}$, $a \neq b$: If $|\Delta a| = 0$, c_{ab} is not defined $\Rightarrow w_a := 0$ and $c_{ab} := 0$. Set the remaining weights accordingly.
4. Set $R^{i+1} := R^i + \Delta V$. Perform this addition iteratively for all vertices, such that updated position $x^{i+1} := x^i + v$ of an individual vertex does not produce self-intersections in the surface. Then R^{i+1} also has no self-intersections.
5. Update $i \leftarrow i + 1$ and return to step (2) if stopping criterion has not been met (same ϵ as in Sec. 2.1). Otherwise, or if a maximum number of iterations has been reached, return.

3 Computation of the Displacement ΔR

The displacement vector field ΔR is computed on the basis of the image data I, after applying a nonlinear isotropic diffusion filter [8]: The filtered image is the solution of the partial differential equation $\partial_t u = \operatorname{div}\left(g(|\nabla u_\sigma|^2)\nabla u\right)$ with $u(x, 0) = I(x)$ and diffusivity function $g(s) = 1 - \exp\left(-3.315(\lambda/s)^4\right)$ for $s > 0$ and $g(s) = 1$ for $s \leq 0$. A displacement vector Δr_k is computed for each vertex k of the surface by analyzing a 1D intensity profile at vertex position x along the (unit) surface normal u. This profile is sampled equidistantly over a length L at the set of points:

$$P = \{x_i := x + [(i-1)/(N_p - 1) - 1/2] \cdot L \cdot u \text{ with } i = 1, \ldots, N_p\}.$$

The result of the analysis will yield the displacement vector $\Delta r_k = w(x_n - x)$, with $x_n \in P$, $n \in \{1, \ldots, N_p\}$ and a confidence weight w, at the vertex k of the surface. Fig. 1 shows some typical profiles in different anatomical regions.

The basic assumptions for the computation of the displacement are based on the following simple *model* for the intensity distribution around the liver boundary: The intensity inside the liver lies in the range $G_L = [g_L - t_L, g_L + t_L]$, where g_L denotes the average liver intensity and t_L the corresponding tolerance. Analogously, the intensity of tumors (potentially) contained in the liver are in the range $G_T = [g_T - t_T, g_T + t_T]$. Furthermore, there exist bounds $g_{\min}$ and $g_{\max} :=$

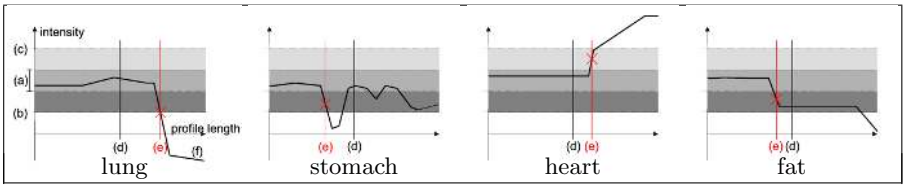

Fig. 1. Exemplary intensity profiles. (a) G_L, (b) $g_{\min}$, (c) $g_{\max}$, (d) current vertex position x, (e) suggested new position x_n, (f) profile plot.

$g_L + 3t_L$ below resp. above which the intensity indicates definitely non-liver and non-tumor tissue. The liver boundary is characterized by a minimal absolute value of the intensity gradient $d_{\min} > 0$. A sample point along a profile is only considered inside the liver/tumor if at least $c_{\min} := N_p/5$ consecutive neighbors on the profile lie within G_L/G_T. Based on these assumptions we propose the following strategy to compute $x_n \in P$ from the intensity profile at a vertex:

1. Initialize $n := (N_p + 1)/2$ and $w := 1$.
2. If $I(x_n) \notin G_L \rightarrow$ Determine largest $i < n$ with $I(x_i) \in G_L$ and set $n := i$. If there is no such point i, set $w := 0$.
3. If $I(x_n) \in G_L \rightarrow$ Count number c of consecutive $i \leq n$ with $I(x_i) \in G_L$. If $c \geq c_{\min}$, define x_n to be inside liver.
4. If x_n outside liver but $I(x_n) \in G_L \rightarrow$ Count number c of consecutive $i \geq 1$ with $I(x_i) \in G_L$. If $c \geq c_{\min}$, set $n := c$ and define x_n to be inside liver.
5. If x_n outside liver $\rightarrow$ Set $w := 0$.
6. If $I(x_n) \notin G_L \rightarrow$ If tumor present, search for an x_i that is inside tumor. Use the same strategy as for the liver, but with G_T instead of G_L. If such an x_i exists, set $n := i$ and $w := 0.75$.
7. If $I(x_n) \notin G_L \cup G_T \rightarrow$ Determine all consecutive $i \leq N_p$ with $I(x_i) < g_{\min}$. If smallest such $i < n$, set $n := i$, $w := 0.75$ and return.
8. If $w = 0 \rightarrow$ Return.
9. Now x_n is either inside liver or inside tumor. The remaining steps are equal in both cases. $\rightarrow$ Find first point $i > n$ with either $|I'(x_i)| > d_{\min}$ or $I(x_i) \notin G_{L/T}$. If $I(x_i) \notin G_{L/T}$, set $n := i - 1$, else $n := i$.
10. If $|I'(x_n)| > d_{\min} \rightarrow$ Find point of inflection x_i with smallest $i > n$, then find largest $j < i$ such that $I(x_j) > g_{\min}$. Set $n := j$.
11. Find largest $i < N_p$ with $I(x_i) < g_{\max}$. If $i < n$, set $n := i$. This prevents from moving too far into regions such as kidney or heart.

4 Estimation of Intensity-based Parameters

The intensity parameters required for computing the displacement field ΔR (c.f. Sec. 3) are estimated based on an analysis of two different histograms H_1 and H_2 of the preprocessed image data. The basic idea is to discriminate the major liver peak(s) from minor yet distinct other peaks, which indicate the presence of tumor

tissue. H_1 is the histogram on the volume inside some given liver surface, while H_2 considers a slightly *enlarged* liver volume by growing the current liver surface by 5 voxels. The histograms are evaluated only on voxels with an intensity in the range of $[0, 300]$ HU, which is assumed to cover both liver and tumor tissue. A weighted sum of 10 Gaussians P_i $(i = 1, \ldots, 10)$ is fitted to each of the two histograms using the Expectation Maximization (EM) algorithm on a Gaussian mixture model. As a result, we obtain weights w_i, means μ_i, standard deviations σ_i and the so-called *peak height* $h_i = w_i/\sigma_i$ for each Gaussian P_i. First, the tumor intensity range G_T is computed based on histogram H_1:

1. Identify P_i in H_1 with the highest h_i. P_i is assumed to model the intensity distribution inside the liver (liver peak).
2. Identify $N := \{j \mid |\mu_i - \mu_j| < \max(15, \min(20, 3\sigma_i)),\ h_j > 0.02 \cdot h_i\}$ as *nearby liver peaks*. Set $l_1 := \min_{j \in N}\{\mu_j - \sigma_j \cdot \max(1, \min(3, 50 \cdot h_j^2/h_i^2))\}$ as the *lower liver boundary*. Set the *upper liver boundary* u_1 accordingly.
3. Compute the *approximate total peak height* as $r := \sum_{j \in N} h_j$. Note that r is not necessarily a peak height of our Gaussian mixture.
4. Now identify *potential tumor peaks* $T := \{j \mid \mu_j < l_1, h_j > 0.05 \cdot r\}$. If $|T| = 0$, assume that there is no big tumor. Otherwise identify $\sigma_{\min} := \min_{j \in T}\{\sigma_j\}$. Set $T^* := T \setminus \{j \in T \mid \sigma_j > 2\sigma_{\min}\}$ and $t := \arg\max_{j \in T^*}\{\mu_j\}$. P_t is assumed to model the intensity distribution inside tumors.
5. Fix the tumor intensity range G_T with $g_T := \mu_t$ and $t_T := \min(20, 3\sigma_t)$.

Since Histogram H_1 possibly excludes important regions of the liver, which are not covered by the current segmentation, we analyze the Gaussians fitted to H_2 in a second step to see whether the liver intensity range needs to be enlarged:

1. Identify liver intensity boundaries l_2 and u_2 in H_2 just like l_1 and u_1 in H_1.
2. Identify a tumor Gaussian P_{t_2} in H_2 just as in H_1. Accept P_{t_2} only if none was found in H_1, and if $\mu_{t_2} > 0.5\,(l_2 + u_2) - 30$. Then set $g_T := \mu_t$ and $t_T := \min(20, 3\sigma_{t_2})$. This reduces the risk of including fat to the liver range.
3. Set $l := l_2$ and $u := \max(u_1, u_2)$. If $l_1 < l_2$ and not $g_T > l_1$, set $l := l_1$.
4. Fix $g_L := 0.5\,(l + u)$ and $t_L := 0.5\,(u - l)$, and $d_{\min} := 0.5\,t_L$.

5 Initialization of Position T^0

It is assumed that the general position of the patient in the CT scanner is known and correct from the DICOM header (e.g. FFS = Feet First Supine). The idea of the position initialization is to robustly detect the lower rim of the right lobe of the lung and to position the liver model below it. First, all connected components with intensity values less than -600 HU are determined and the largest two components (left and right lobe), which are adjacent to the upper border of the image volume, are selected. Next, the lobe component on the right-hand side is projected in patient axis direction from feet to head and the center and orientation of the resulting lung area is determined. The liver model is now translated and oriented according to the back-projected center point and orientation of the lower rim of the right lobe.

6 Segmentation Algorithm

The segmentation algorithm consists of a series of steps combining the methods presented in the sections above, see Tab. 1. Each step is one of the following methods: position initialization (**Init**, see Sec. 5), parameter estimation (**Estimate**, see Sec. 4), optimization of the shape model (**Opt-SSM**, see Sec. 2.1), constrained free-form deformation (**Opt-CFFD**, see Sec. 2.2) or some other processing step explained in the table. For each step the parameters for the specific method or other comments are listed in the third column labeled *details*.

7 Results and Conclusions

We presented an algorithm for automatic segmentation of the liver in CT data. Its main components are statistical shape and constrained free-form deformations, which can directly be applied to other segmentation problems as well. The computation of the displacement *forces* and the estimation of parameters were designed to solve the liver segmentation problem. Yet, it may be used to solve other segmentation problems, where our simple intensity model applies.

The statistical liver model was generated from 43 different data sets and has $m \approx 12000$ vertices. Refer to [7] for details about the training data. Comparisons to manual segmentations were performed on 10 liver datasets provided by the MICCAI 2007 *Workshop on 3D Segmentation in the Clinic* [9]. Fig. 2 and Tab. 2

Step	Type	Details
1	**Preproc.**	two passes of nonlinear diffusion filtering of I with $t = 25$, $\Delta t = 5$, $\lambda = 10$. Pass 1 with $\sigma = 3$, and pass 2 with $\sigma = 1$.
2	**Init**	position T^0
3	**Estimate**	compute $G_L, G_T, d_{\min}$
4	**Opt-SSM**	only position (rigid + isotropic scaling $\in [0.5, 1.5]$), $L := 50$ mm, $N_p := 50$, $g_{\min} := 0$
5	**Estimate**	recompute $G_L, G_T, d_{\min}$
6	**Opt-SSM**	position and shape parameters (10 modes), $L := 60$ mm and $N_p := 60$ without tumor, $g_{\min} := 0$, $\epsilon := 0.1$ mm
7	**Estimate**	recompute $G_L, d_{\min}$ only
8	**Opt-SSM**	position and shape parameters (43 modes), $g_{\min} := g_L - 3t_L$ without tumor and $g_T - t_T$ with tumor, $\epsilon := 0.05$ mm
9	**Estimate**	recompute $G_L, d_{\min}$ only
10	**Opt-SSM**	same as step 7 but with $L := 40$ mm and $N_p := 40$ with tumor
11	**Opt-SSM**	Only performed if no tumor: $L := 20$ mm, $N_p := 40$.
12	**Remeshing**	The surface of the SSM is scan-converted, interior holes are filled, a new surface mesh is generated as input for the following steps.
13	**Opt-CFFD**	narrow band radius $r_B := 10$ mm, $L := 30$ mm, $N_p := 60$, $\epsilon := 0.03$ mm, maximum number of iterations := 50.
14	**Opt-CFFD**	Only performed if no tumor was detected: $L := 10$ mm, $N_p := 50$, otherwise same as last OPT-CFFD step.

Table 1. Segmentation algorithm. Parameters remain the same if not noted otherwise.

show qualitative and quantitative results. The not yet optimized run-time of the algorithm was 15 minutes per liver on an Intel 3.2 GHz processor. The overall performance of our method has a *score* of 73 (see [9]). There has been no failure.

Segmentation errors sometimes occur at regions where anatomical structures with very similar intensity values are located close to the liver, in particular if parts of those structures can be captured within a typical liver shape: lower part of vena cava (Fig. 2 top, right), duodenum (Fig. 2 middle, right), heart, muscles, stomach and pancreas. The consideration of tumors inside the liver during the segmentation process (see Sec. 3) is very important and works very well (Fig. 2 middle and bottom row). At high noise levels in the original image data the isotropic nonlinear diffusion process is stopped before reaching the liver boundary (e.g. case 2). Some deviations are caused by incorrect manual segmentations (e.g. Fig. 2 middle row, middle column, near the gallbladder).

The initiative of providing a common pool of test data as well as well-defined measures for evaluation is indispensable for further progress in the field of automatic image segmentation. Yet it remains difficult to establish the correct ground truth, especially for the liver, due to the difficulty to clearly define the exact boundary of the liver tissue (e.g. at the inner side, where the portal vein enters the liver or the vena cava). Although fully automatic liver segmentation algorithms are desirable in the clinical routine, methods that reduce and facilitate manual interaction will remain essential in case of failures.

Acknowledgments. D. Kainmüller is supported by DFG Collaborative Research Center SFB 760, H. Lamecker by the DFG Research Center MATHEON.

References

1. Montagnat, J., Delingette, H.: Volumetric medical images segmentation using shape constrained deformable models. In: CVRMed. (1997) 13–22
2. Cootes, T., Hill, A., Taylor, C., Haslam, J.: Use of active shape models for locating structures in medical images. Image and Vision Computing **12** (1994) 355–366
3. Weese, J., Kaus, M., Lorenz, C., Lobregt, S., Truyen, R., Pekar, V.: Shape constrained deformable models for 3d medical image segmentation. In Insana, M., Leahy, R., eds.: IPMI. Volume 2082 of LNCS., Springer-Verlag (2001) 380–387
4. Heimann, T., Münzing, S., Meinzer, H.P., Wolf, I.: A shape-guided deformable model with evolutionary algorithm initialization for 3d soft tissue segmentation. In: IPMI 2007. Volume 4584 of LNCS., Springer-Verlag (2007) 1–12
5. Heimann, T., Wolf, I., Meinzer, H.P.: Active shape models for a fully automated 3d segmentation of the liver - an evaluation on clinical data. In Larsen, R., Nielsen, M., Sporring, J., eds.: MICCAI. Volume 4191 of LNCS., Springer-Verlag (2006) 41–48
6. Lamecker, H., Lange, T., Seebaß, M.: A statistical shape model for the liver. In Dohi, T., Kikinis, R., eds.: MICCAI. Volume 2489 of LNCS., Springer (2002) 422–427
7. Lamecker, H., Lange, T., Seebaß, M.: Segmentation of the liver using a 3d statistical shape model. Technical report, Zuse Institute Berlin (2004)
8. Weickert, J., ter Haar Romeny, B.M., Viergever, M.A.: Efficient and reliable schemes for nonlinear diffusion filtering. IEEE Trans. Image Proc. **7**(3) (1998) 398–410
9. Heimann, T., van Ginneken, B., Styner, M.: Miccai workshop on 3d segmentation in the clinic (2007) http://mbi.dkfz-heidelberg.de/grand-challenge2007/.

Dataset	Overlap Error		Volume Diff.		Avg. Dist.		RMS Dist.		Max. Dist.		Total
	[%]	Score	[%]	Score	[mm]	Score	[mm]	Score	[mm]	Score	Score
1	6.3	76	-2.3	88	0.9	77	2.0	73	20.6	73	77
2	11.5	55	-10.8	43	1.6	60	2.4	66	17.0	78	60
3	4.7	82	-1.6	91	0.9	77	2.0	72	21.4	72	79
4	7.2	72	-0.5	98	1.2	70	2.4	67	18.4	76	76
5	8.8	66	-6.1	68	1.5	62	2.5	65	21.5	72	66
6	7.0	73	-5.6	70	1.3	68	3.3	54	36.5	52	63
7	6.3	76	-1.9	90	1.1	74	3.1	57	25.6	66	73
8	4.5	82	-0.2	99	0.7	82	1.5	79	13.5	82	85
9	4.1	84	-1.0	95	0.5	88	1.0	86	15.9	79	86
10	9.2	64	-5.7	70	1.3	67	2.3	68	19.1	75	69
Average	7.0	73	-3.6	81	1.1	72	2.3	69	20.9	72	73

Table 2. Results of the comparison metrics and scores for all ten test cases.

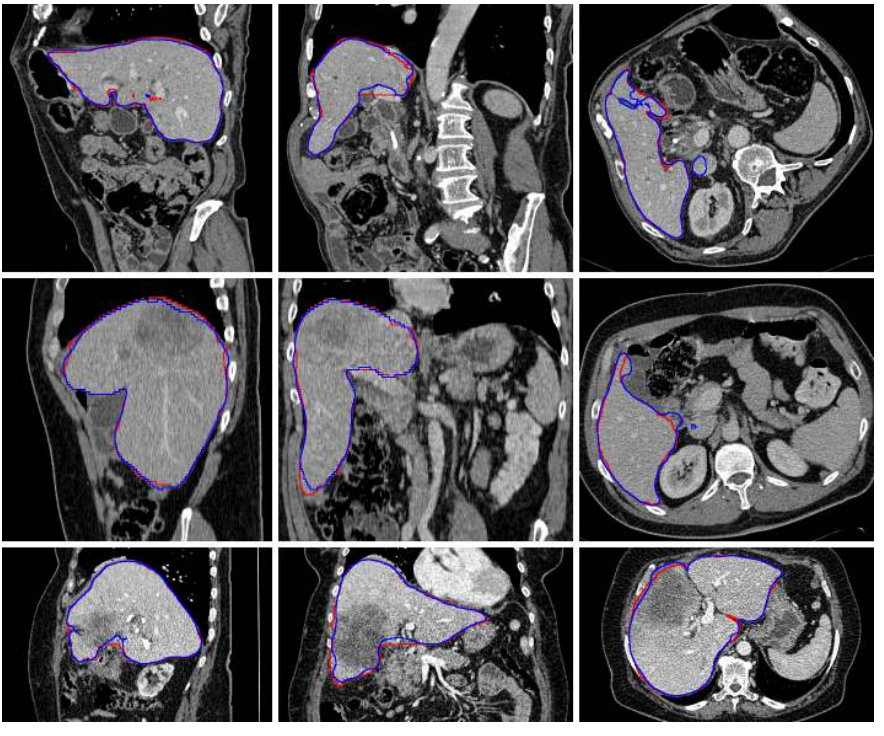

Fig. 2. From left to right, a sagittal, coronal and transversal slice from a relatively easy case (1, top), an average case (4, middle), and a relatively difficult case (3, bottom). The outline of the reference standard segmentation is in red, the outline of the segmentation of the method described in this paper is in blue. Slices are displayed with a window of 400 and a level of 70.